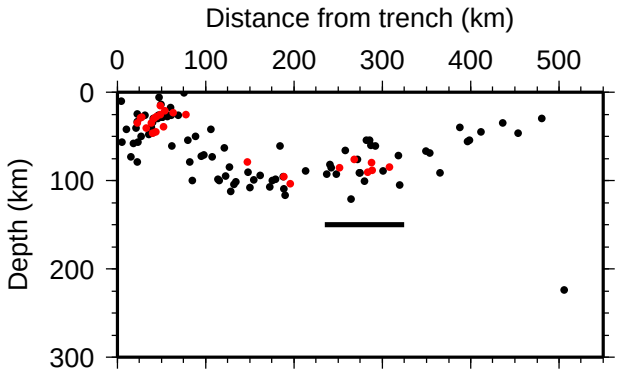

Figure S1. Trench-normal cross-section of seismicity from the 1960–2013 ISC Bulletin event catalog (International Seismological Centre 2011) (black dots) in bin 3 of Fig. 5. Hypocenter locations for earthquakes from the relocated 1960–2008 EHB Bulletin event catalog (International Seismological Centre 2011) (red dots) are shown for reference. A black horizontal bar marks the location of the shallower cluster of seismicity centered at ∼14°S, 72.85°W that was noted for Fig. 3.

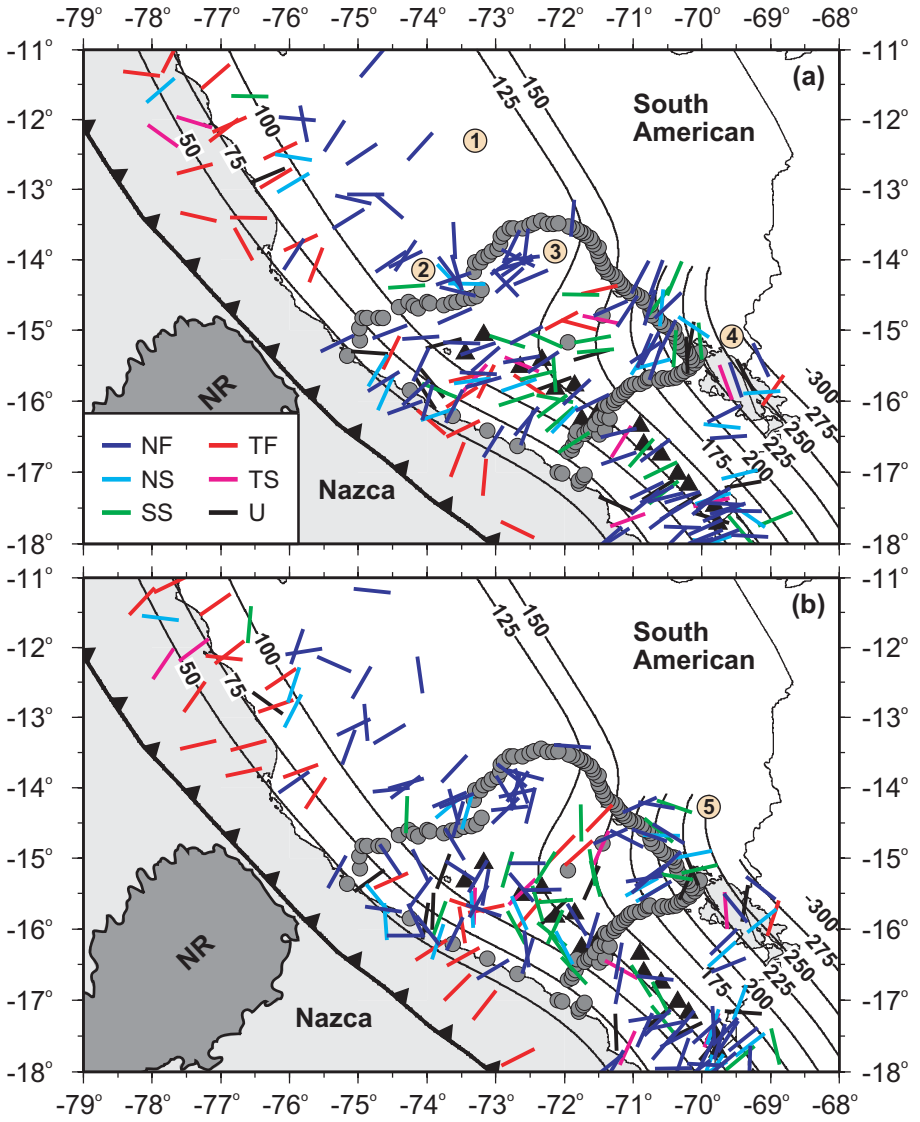

Figure S2. (a) T and (b) P axis orientations (line segments) for intermediate depth earthquakes from the 1976–2013 GCMT catalog (Dziewonski et al. 1981; Ekström et al. 2012) (see Fig. 4 for corresponding focal mechanisms). Axis orientations are colored by faulting type following the classification of Zoback (1992), which is based on the plunge of P, T, and B axes. The faulting types include normal faulting (NF), predominately normal with strike-slip component (NS), strike-slip faulting (SS), predominately thrust with strike-slip component (TS), thrust faulting (TF), and unknown (U). The unknown faulting type describes events which do not clearly fit into any of the other categories and generally applies to smaller and/or less well constrained focal mechanisms (Zoback 1992). The majority (69%) of events below ∼80 km depth exhibit normal (NF or NS) mechanisms. Circled numbers mark regions of interest discussed in the text. (1) Normal faulting events primarily exhibit downdip extension in the horizontal subduction region to the northwest. (2) A cluster of seismicity centered at ∼14.25°S, 73.5°W is comprised of normal faulting mechanisms showing mainly NW-SE extension. (3) A cluster of shallower seismicity near the PG line, centered at ∼14°S, 72.85°W, consists of normal faulting events at various orientations, including those that signify N-S and NW-SE extension. (4) Normal faulting mechanisms located near the intersection of the PE and PF lines and slightly to the southeast between the 225-km and 275-km isodepth contours indicate NNW-SSE extension. (5) Several thrust and oblique faulting events are located within a linear ENE-WSW-oriented concentration of events along the sharp bend in isodepth contours (coast to 225-km contour), especially between the 125-km and 150-km isodepth contours. The P axis orientations of some of these events show N-S and NW-SE compression. Other symbols and structures are as in Figs 1 and 3.

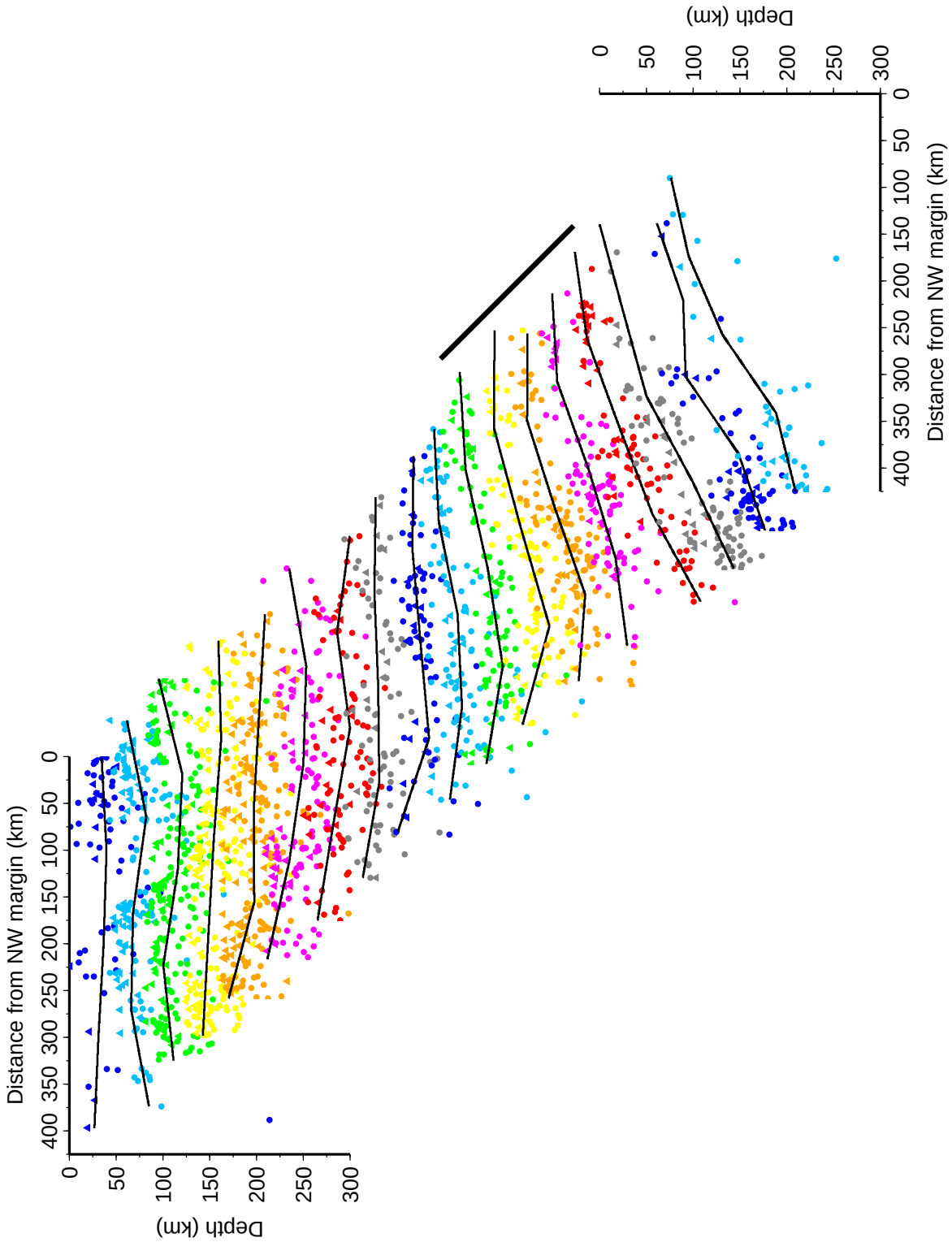

Figure S3. Perspective view (updip) of cross-sections of slab seismicity from the ISC (dots) and EHB (triangles) catalogs in trench-parallel bins h1 (top) to h18 (bottom; see Fig. 6 for bin locations). Events within the overriding plate are not shown. All events within a particular bin are shown as a single color. Variations in color between bins are used to distinguish cross-sections. Weighted piecewise-linear regression fits to the slab seismicity in each cross-section are shown (black lines). Cross-sections for bins h11–h15 shown in Fig. 7 are marked by a heavy black line. Note the abrupt step in the fit for bin h17 due to a poorly constrained regression from sparse data in this bin. See Fig. S4 of the auxiliary material for plots of individual cross-sections.

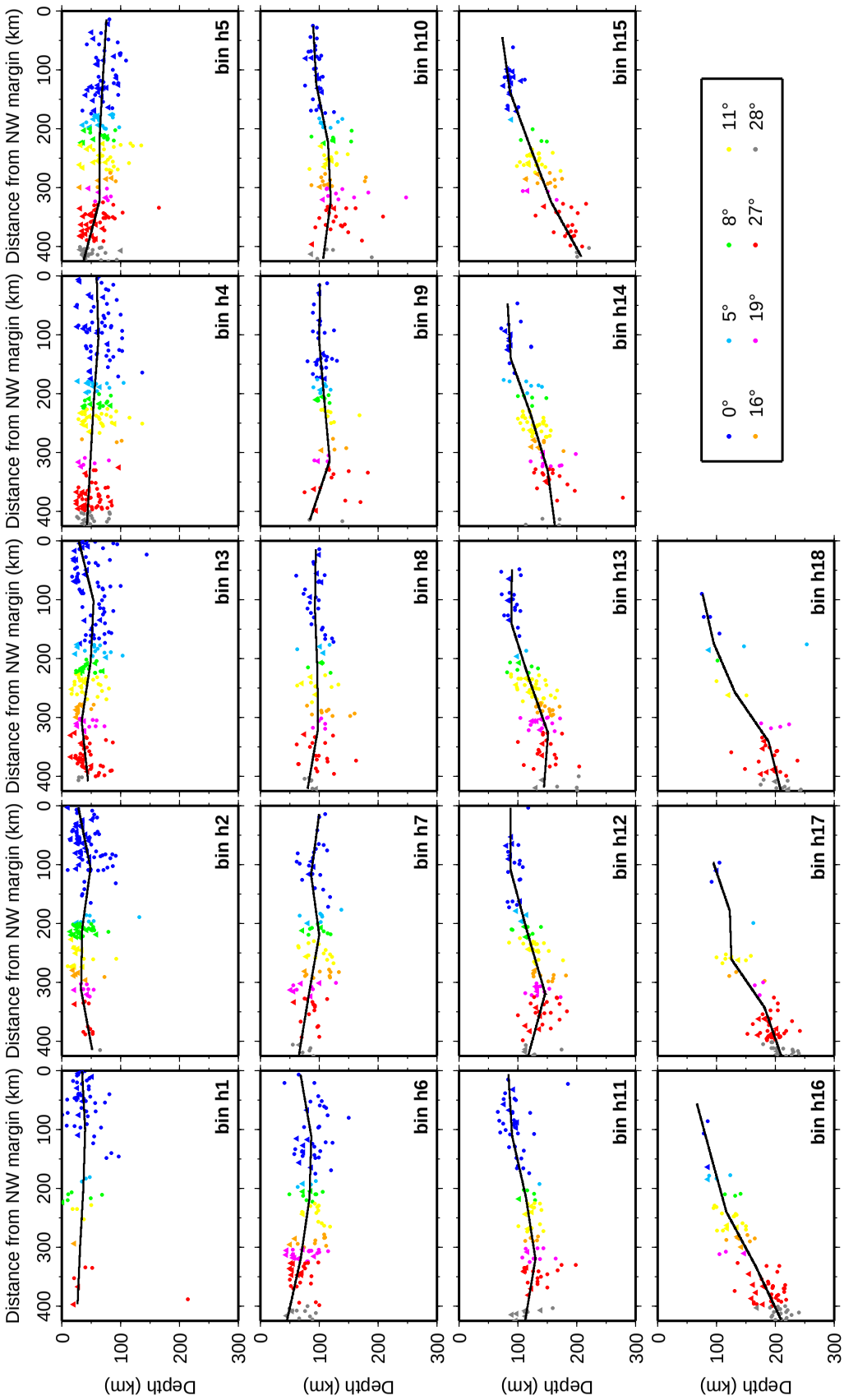

Figure S4. Individual cross-sections of slab seismicity from the ISC (dots) and EHB (triangles) catalogs in trench-parallel bins h1 to h18 (see Fig. 6 for bin locations). Events within the overriding plate are not shown. Hypocenter locations are colored to reflect slab dip as estimated in Fig. 5. Weighted piecewise-linear regression fits to the slab seismicity in each cross-section are shown (black lines). Cross-sections for bins h11-h15 shown in Fig. 7 are located in the third row from the top. Note the abrupt step in the fit for bin h17 due to a poorly constrained regression from sparse data in this bin.

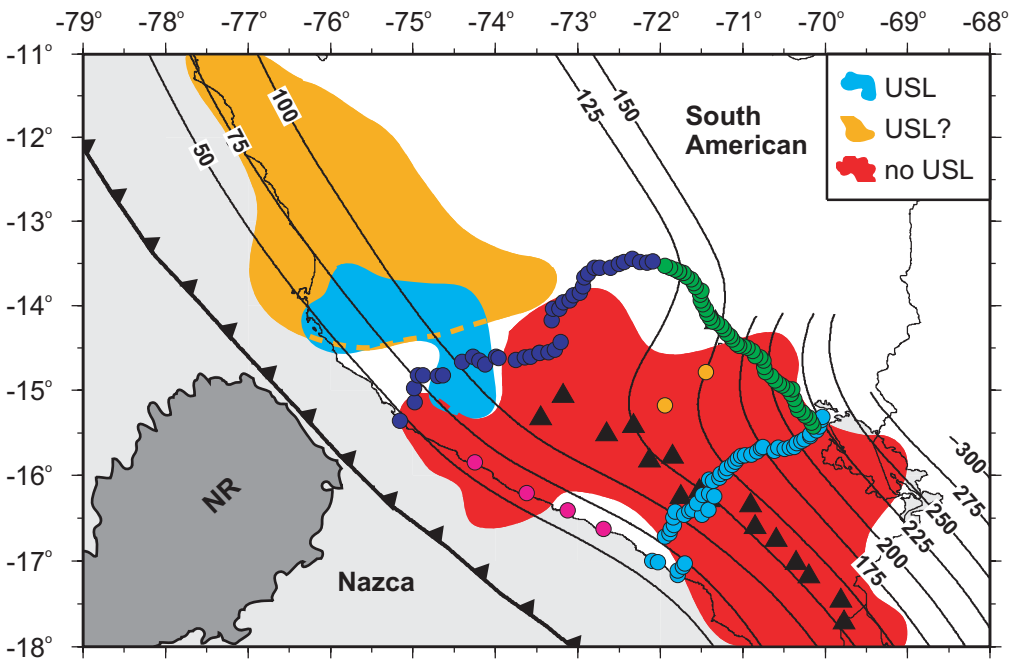

Figure S5. Mapping the lateral extent of the USL using PeruSE P waveforms. Shaded contours of USL (blue), possible USL (orange), and no USL (red) zones are shown. These zones are based on event locations in Fig. 10. Other symbols and structures are as in Figs 1 and 3.

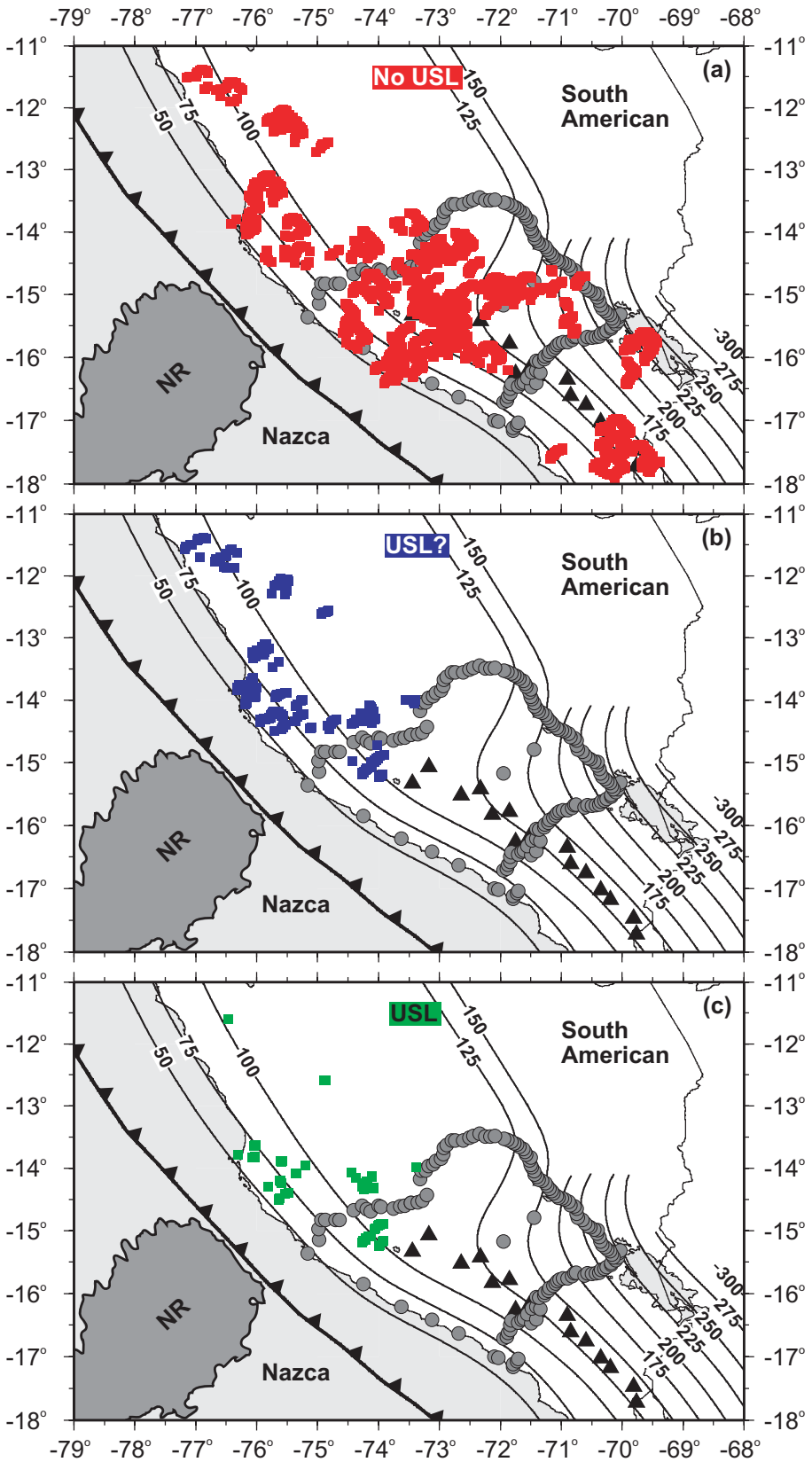

Figure S6. Approximate locations of S-to-P conversion points from the top of the Nazca slab for waveforms recorded at PeruSE stations. Conversion points for waveforms which indicated (a) no USL is present, (b) possible USL presence, and (c) USL is present are shown. Compare the locations of these conversion points to the zones in Fig. S5 of the auxiliary material. Other symbols and structures are as in Figs 1 and 3.